bioRxiv preprint doi: https://doi.org/10.1101/2020.02.17.952218; this version posted February 18, 2020. The copyright holder for this preprint (which was not certified by peer review) is the author/funder, who has granted bioRxiv a license to display the preprint in perpetuity. It is made available under aCC-BY-NC-ND 4.0 International license.

The effects of microcystin-LR in *Oryza sativa* root cells: F-actin as a new target of cyanobacterial toxicity

D. Pappas, S. Gkelis, E. Panteris*

Department of Botany, School of Biology, Aristotle University of Thessaloniki, 541 24 Thessaloniki, Greece

* Correspondence to: E. Panteris, e-mail: epanter@bio.auth.gr

Keywords: Actin filaments; Cell cycle; Endoplasmic reticulum; Golgi apparatus; *Microcystis*; Rice

bioRxiv preprint doi: https://doi.org/10.1101/2020.02.17.952218; this version posted February 18, 2020. The copyright holder for this preprint (which was not certified by peer review) is the author/funder, who has granted bioRxiv a license to display the preprint in perpetuity. It is made available under aCC-BY-NC-ND 4.0 International license.

ABSTRACT

- Microcystins are toxins produced by cyanobacteria, notorious for negatively affecting a wide range of living organisms, among which several plant species. Although microtubules are a well-established target of microcystin toxicity, its effect on filamentous actin (F-actin) in plant cells has not been studied yet.
- The effects of microcystin-LR (MC-LR) and the extract of a microcystin-producing freshwater cyanobacterial strain (*Microcystis flos-aquae* TAU-MAC 1510) on the cytoskeleton (F-actin and microtubules) of *Oryza sativa* (rice) root cells, were studied by light, confocal, and transmission electron microscopy. Considering the role of F-actin in endomembrane system distribution, the endoplasmic reticulum and the Golgi apparatus in extract-treated cells were also examined.
- F-actin in both MC-LR- and extract-treated meristematic and differentiating root cells exhibited time-dependent alterations, ranging from disorientation and bundling to the formation of ring-like structures, eventually resulting to a collapse of the F-actin network at longer treatments. Disorganization and eventual depolymerization of microtubules, as well as abnormal chromatin condensation were observed following treatment with the extract, effects which could be attributed to microcystins and other bioactive compounds. Moreover, cell cycle progression was inhibited in extract-treated roots, specifically affecting the mitotic events. As a consequence of F-actin network disorganization, endoplasmic reticulum elements appeared stacked and diminished, while Golgi dictyosomes appeared aggregated.
- These results support that F-actin is a prominent target of MC-LR, both in pure form and as an extract ingredient. Endomembrane system alterations

bioRxiv preprint doi: https://doi.org/10.1101/2020.02.17.952218; this version posted February 18, 2020. The copyright holder for this preprint (which was not certified by peer review) is the author/funder, who has granted bioRxiv a license to display the preprint in perpetuity. It is made available under aCC-BY-NC-ND 4.0 International license.

55 can also be attributed to the effects of cyanobacterial bioactive compounds
56 (including microcystins) on F-actin cytoskeleton.
57

58 **INTRODUCTION**

59 Cyanobacteria are photosynthetic, oxygenic prokaryotes, inhabiting a variety of
60 aquatic and terrestrial environments, surviving even extreme conditions (such as high
61 temperature or salinity etc.; Codd et al., 2017). A wide range of species are known to
62 produce cyanotoxins, a group of chemically diverse secondary metabolites (as
63 reviewed by Pantelić et al., 2013), proven to be harmful to higher eukaryotes,
64 including humans (Buratti et al., 2017) and various plant species (Máthé et al., 2013;
65 Mitrovic et al., 2004). The most common cyanotoxins found in freshwater bodies are
66 microcystins (MCs), water-soluble monocyclic heptapeptides, exhibiting two variable
67 amino acids (Catherine et al., 2017). The toxicity of MCs is due to their ability to
68 inhibit the activity of protein phosphatases 1 (PP1) and 2A (PP2A) (MacKintosh et al.,
69 1990), which are involved in the cell cycle progression (Brautigan and Shenolikar,
70 2018).
71 MCs are released into the surrounding water during cyanobacterial cell lysis (Sivonen
72 and Jones, 1999), thus becoming eventually accessible to consumers either directly
73 (through water supply) or indirectly, affecting crops (through irrigation water) destined
74 for consumption. When present in irrigation water (due to naturally occurring
75 cyanobacteria in freshwaters), MCs have been shown to bioaccumulate in cultivated
76 plant species (Corbel et al., 2016; Drobac et al., 2017), raising serious concerns over
77 food safety and the impacts on consumers' health (Cao et al., 2018a).
78 Rice (*Oryza sativa* L.) is a crop of great commercial value worldwide (FAO, 2018).
79 Since its cultivation is closely related to the aquatic environment, it is prone to all the
80 dangers imposed by the presence of cyanobacteria in the surrounding water.
81 Although many studies have focused on the accumulation and toxicity of MCs in rice
82 (Azevedo et al., 2014; Chen et al., 2012; Liang et al., 2016), their effects on the

bioRxiv preprint doi: https://doi.org/10.1101/2020.02.17.952218; this version posted February 18, 2020. The copyright holder for this preprint (which was not certified by peer review) is the author/funder, who has granted bioRxiv a license to display the preprint in perpetuity. It is made available under aCC-BY-NC-ND 4.0 International license.

physiology of rice cells remain unclear. A recent study has underlined the negative effects of MC-contaminated water on rice root growth (Cao et al., 2018b), as a result of mitotic disruption in dividing root cells.

Previous studies on plant cells have shown that MCs disrupt microtubule organization, leading to mitotic abnormalities, and induce chromatin hypercondensation, due to histone H3 hyperphosphorylation, while alterations in cell cycle progression have also been reported (for a review on the effects of MCs, see Máthé et al., 2013). Even though chromatin and microtubules are well-known "targets" of MCs in plant cells, the other component of the plant cytoskeleton, F-actin, has not been studied in MC-treated cells of any plant species so far. However, F-actin is important for plant growth, regulating the intracellular distribution of several organelles (Volkmann and Baluška, 1999) and driving cytoplasmic streaming, a function pivotal for plant cell viability (Shimmen and Yokota, 2004). All reports about the adverse effects of MCs on plant cytoskeleton have been based on applying purified MCs (e.g. Garda et al., 2016; Máthé et al., 2013), as purified toxins offer high precision in determining the exact concentrations. On the other hand, crude extracts of MC-producing cyanobacterial strains, known to negatively affect plant growth, are helpful in simulating the natural exposure of plants to MCs during lab experiments (Pflugmacher et al., 2007; Prieto et al., 2011). In accordance, in the present study, the effects of both purified microcystin-LR (MC-LR) and a toxic cyanobacterial extract (containing MCs) on F-actin of rice root cells were investigated. In order to further highlight the significance of any disruption of F-actin due to the toxic extract, endoplasmic reticulum and Golgi apparatus distribution, related to F-actin (Boevink et al., 1998), as well as cytoplasmic streaming (Shimmen and Yokota, 2004; Volkman and Baluška, 1999) were examined.

MATERIALS AND METHODS

Cyanobacterial strains, growth media and culture conditions

bioRxiv preprint doi: https://doi.org/10.1101/2020.02.17.952218; this version posted February 18, 2020. The copyright holder for this preprint (which was not certified by peer review) is the author/funder, who has granted bioRxiv a license to display the preprint in perpetuity. It is made available under aCC-BY-NC-ND 4.0 International license.

A strain of the TAU-MAC culture collection (Gkelis and Panou, 2016), *Microcystis flos-aquae* TAU-MAC 1510, isolated from Lake Pamvotis, Greece (Gkelis et al., 2015a), was used for experimental purposes. *Microcystis flos-aquae* TAU-MAC 1510 has been found to be toxic (Gkelis et al., 2015a), producing a range of microcystins, including MC-YR, MC-LR, [D-Asp^3] MC-LR and MC-HilR (Gkelis et al., 2019). The strain was cultured in BG-11 medium, containing $NaNO_3$ (Rippka, 1988), in a 500 mL glass Erlenmeyer flask (250 mL of medium were inoculated with a 4-5 mL inoculum, from an exponentially growing pre-culture, under aseptic conditions). The culture was grown at 24±1ºC for about 30 days in a 12 h:12 h light:dark cycle at a photosynthetic photon flux density of 10 μmol m^{-2} s^{-1} using cool white fluorescent lamps.

Biomass collection and extraction

The culture was centrifuged at 3,500 rpm for 10 min. The supernatant was discarded and the precipitate (biomass) was stored at -70ºC overnight. Frozen biomass was lyophilized with an ALPHA 1-4 freeze dryer (Martin Christ, Gefriertrocknungsanlagen, Osterode am Harz, Germany), at temperature ranging from -48ºC to -54ºC and pressure between 0.05 and 0.02 mbar, until dry. Dry biomass was weighed (150 mg) and extracted thrice in 21 mL of 75% (v/v) methanol in glass tubes. The sample was sonicated during the first extraction step for 10 min with a Vibra-Cell VC-300 High Intensity Ultrasonic Processor (Sonics and Materials Inc., Newtown, CT, USA) and stirred for 45 min at each extraction step at room temperature. The extract was left to evaporate under aseptic conditions and the pellet was resuspended in 5 mL of double-distilled water. The aqueous extract was filtered through Whatman Polydisc TF filters (Whatman plc, Little Chalfont, UK) with a pore size of 0.2 μm.

Plant material and exposure to MC-LR and the crude extract

Rice (*Oryza sativa* cv Axios, kindly provided by the National Cereal Institute, Thessaloniki, Greece) seeds were germinated on filter paper moistened with tap

bioRxiv preprint doi: https://doi.org/10.1101/2020.02.17.952218; this version posted February 18, 2020. The copyright holder for this preprint (which was not certified by peer review) is the author/funder, who has granted bioRxiv a license to display the preprint in perpetuity. It is made available under aCC-BY-NC-ND 4.0 International license.

water, in the dark, at 24±1°C. MC-LR purified from *Anabaena* strains (Halinen et al., 2007), generously provided by Prof. Kaarina Sivonen (Department of Microbiology, University of Helsinki), was used for treatments. Four- to five-day-old seedlings were placed with their roots submerged in either cyanobacterial aquatic extract or an aquatic solution of MC-LR inside Eppendorf tubes for various time periods (30 min, 1, 2, 3 or 24 h) at the same conditions. Seedlings submerged in tubes with distilled water were used as control. The concentration of the MC-LR aquatic solution was set at 45 $\mu g \cdot mL^{-1}$, equal to the total concentration of microcystins contained in the *Microcystis flos-aquae* TAU-MAC 1510 strain (Gkelis et al., 2019), in order to achieve comparable results. Following exposure, root tips 2-3 mm long were cut with steel razor blades and prepared for fluorescence and transmission electron microscopy (TEM). All chemicals and reagents were purchased from Applichem (Darmstadt, Germany), Sigma-Aldrich (Taufkirchen, Germany) and Merck (Darmstadt, Germany) and all experimental procedures described below were performed at room temperature, unless otherwise stated.

Endoplasmic reticulum and tubulin immunolabeling

Endoplasmic reticulum and tubulin immunostaining were performed as mentioned by Adamakis et al. (2016), with some modifications. In particular, root tips were fixed in 4% (w/v) paraformaldehyde (PFA) solution in PEM buffer (50 mM PIPES, 5mM EGTA, 5 mM $MgSO_4$, pH 6.8) with the addition of 5% (v/v) dimethyl sulfoxide (DMSO) for 1 h. Fixed specimens were washed with PEM (3 x 10 min) and cell walls were digested with 2% (w/v) Macerozyme R-10 + 2% (w/v) cellulase Onozuka R-10 (Duchefa Biochemie, Haarlem, Netherlands) solution in PEM for 1 h. After washing with PEM (3 x 10 min), the root tips were squashed on poly-L-lysine-coated coverslips, left to dry, and the cells were extracted with a 5% (v/v) DMSO + 1% (v/v) Triton X-100 solution in phosphate-buffered saline (PBS, pH 7.2) for 1 h. For endoplasmic reticulum immunolabeling, mouse anti-HDEL antibody (2E7, Santa Cruz

bioRxiv preprint doi: https://doi.org/10.1101/2020.02.17.952218; this version posted February 18, 2020. The copyright holder for this preprint (which was not certified by peer review) is the author/funder, who has granted bioRxiv a license to display the preprint in perpetuity. It is made available under aCC-BY-NC-ND 4.0 International license.

Biotechnology, Dallas, TX, USA), diluted 1:50 in PBS, and AlexaFluor488-anti-mouse (Invitrogen, Carlsbad, CA, USA), diluted 1:150 in PBS, were used. For tubulin immunolabeling, rat anti-*α*-tubulin (YOL 1/34, Serotec, Kidlington, UK) was applied as primary antibody and incubated overnight, then washed with PBS and incubated with FITC-anti-rat at 37°C for 3 h. Both antibodies were diluted 1:40 in PBS. DNA was counterstained with DAPI (0.9 mM stock solution of 4',6-diamidino-2-phenylindole in DMSO and further diluted 1:1000 in PBS) for 5 min. After final wash with PBS, all specimens were mounted with an anti-fade medium [PBS 1: 2 glycerol (v/v) + 0.5 % (w/v) p-phenylenediamine].

F-actin labeling with phalloidin

F-actin labeling with fluorescent phalloidin was performed according to Stavropoulou et al. (2018). In short, F-actin in root tips was pre-stabilized in 300 μM *m*-maleimidobenzoyl-*N*-hydroxysuccinimide ester in PEM, with the addition of 0.1% (v/v) Triton X-100 for 30 min in the dark. Immediately after pre-stabilization, fixation was performed with 4% (w/v) PFA in PEM + 5% (v/v) DMSO + 0.1% (v/v) Triton X-100, while DyLight 554-phalloidin (Cell Signaling Technology, Danvers, MA, USA) 1:400 was also added in the fixative for better F-actin preservation. After washing with PEM (3 x 10 min), the specimens were extracted in 5% (v/v) DMSO + 1% (v/v) Triton X-100 in PBS for 1 h and F-actin labeling was performed by incubating with DyLight 554-phalloidin diluted 1:40 in PBS + 0.1% (v/v) Triton X-100 at 37°C for 2 h in the dark. After DNA counterstaining with DAPI (as mentioned above) and washing with PBS, all specimens were mounted with anti-fade medium.

Confocal fluorescence microscopy

Fluorescent specimens were observed with a Zeiss Observer.Z1 (Carl Zeiss AG, Munich, Germany) microscope, equipped with the LSM780 confocal laser scanning

bioRxiv preprint doi: https://doi.org/10.1101/2020.02.17.952218; this version posted February 18, 2020. The copyright holder for this preprint (which was not certified by peer review) is the author/funder, who has granted bioRxiv a license to display the preprint in perpetuity. It is made available under aCC-BY-NC-ND 4.0 International license.

(CLSM) module, with the appropriate filters for each fluorophore. Imaging was achieved with ZEN2011 software according to the manufacturer's instructions.

Fluorescence intensity measurements

Fluorescence intensity measurements for F-actin were performed in maximum intensity projections of serial CLSM sections of root tips (in the meristematic and differentiation zone), treated with 45 $\mu g \cdot mL^{-1}$ MC-LR or the cyanobacterial extract for various time periods (30 min, 1, 2 or 24 h), using ImageJ (https://imagej.net/Fiji), according to Adamakis et al. (2014) and Mylona et al. (2020). The corrected total cell fluorescence (CTCF; Gavet and Pines, 2010) was calculated with the formula: CTCF = Integrated Density – (Area of selected cell X Mean fluorescence of background readings). Thirty individual cells from three different roots per treatment were measured for fluorescence intensity. Results were statistically analyzed (ANOVA with Dunnett's test) using SigmaPlot (San Jose, CA, USA), with significance at $P < 0.001$.

Cell cycle analysis

To assess the frequency of cells in various cell cycle stages, control and treated specimens prepared for F-actin labeling or tubulin immunostaining and DAPI staining were examined under a Zeiss AxioImager.Z2 light microscope equipped with epifluorescence or a Zeiss Observer.Z1 (Carl Zeiss AG, Munich, Germany) microscope with CLSM module. Cells at different cell cycle stages (interphase, preprophase/prophase, metaphase/anaphase and cytokinesis) were recognized according to F-actin/microtubule arrangement and/or chromatin state. At least 1000 individual cells from three different roots per treatment (a minimum of 300 meristematic cells per root) were counted. Statistical analysis of data (chi-squared test, df = 3) was performed with SigmaPlot, with significance at $P < 0.001$.

Live imaging of cytoplasmic streaming

bioRxiv preprint doi: https://doi.org/10.1101/2020.02.17.952218; this version posted February 18, 2020. The copyright holder for this preprint (which was not certified by peer review) is the author/funder, who has granted bioRxiv a license to display the preprint in perpetuity. It is made available under aCC-BY-NC-ND 4.0 International license.

For cytoplasmic streaming recording, 4- to 5-day-old rice seedlings were placed on glass slides and their roots were dipped either in water (control) or in the extract, covered with a coverslip and observed with DIC optics under a Zeiss AxioImager.Z2 light microscope (Carl Zeiss AG), equipped with an AxioCam MRc5 camera (Carl Zeiss AG). Time lapse images were captured using AxioVision Rel. 4.8.2 software (Carl Zeiss AG). Specifically, for each recording, 60 images captured every 2 sec, were combined in videos of 12 sec duration. The extract used for treatment was replenished regularly after each image capture.

Transmission Electron Microscopy (TEM)

Control and extract-treated (for 30 min or 1 h) root tips of 4- to 5-day-old rice seedlings were fixed in 3% (v/v) glutaraldehyde (PolySciences, Niles, IL, USA) in 50 mM sodium cacodylate buffer (pH 7) for 4 h, washed and post-fixed with 1% (w/v) osmium tetroxide in the same buffer for 3 h at 4°C in the dark. Dehydration was performed in an acetone series, followed by treatment with propylene oxide (SERVA, Heidelberg, Germany) at 4°C and embedding in Spurr's resin (PolySciences, Niles, IL, USA). The embedded specimens were sectioned with a Reichert-Jung Ultracut E (Reichert-Jung Optical Company, Vienna, Austria) ultramicrotome. Ultrathin sections (70-90 nm) were collected on formvar-coated copper grids and double-stained in the dark with 2% (w/v) uranyl acetate in 70% (v/v) ethanol for 15 min and 1% (w/v) lead citrate for 10 min. The sections were examined with a JEOL JEM 1011 (JEOL Ltd., Tokyo, Japan) TEM, equipped with a Gatan ES500W (Gatan Inc., Pleasanton, CA, USA) digital camera and images were acquired using Digital Micrograph 3.11.2 software. CLSM and TEM images were processed with Adobe Photoshop CS4 with only linear settings.

RESULTS

Effects on F-actin

bioRxiv preprint doi: https://doi.org/10.1101/2020.02.17.952218; this version posted February 18, 2020. The copyright holder for this preprint (which was not certified by peer review) is the author/funder, who has granted bioRxiv a license to display the preprint in perpetuity. It is made available under aCC-BY-NC-ND 4.0 International license.

Fine actin filaments were abundant in all untreated meristematic cells (Fig. 1A1). F-actin phragmoplasts were obvious in cytokinetic cells, either control or treated with MC-LR for various times (arrows in Fig. 1). In MC-LR-treated cells, cortical actin filaments appeared disoriented (indicative arrowheads in Fig. 1B2) and bundled (indicative arrowheads in Figs 1C2, D2), from 30 min until 2 h of exposure, compared to the control (Fig. 1A2). Especially after 30 min and 1 h, ring-shaped F-actin conformations (typical examples in Fig. 1C4) could be observed in affected meristematic cells (arrowheads in Figs 1B3, C3, C5). However, after 24 h of treatment, F-actin intensity deteriorated significantly (Fig. 1E1) and cortical actin filaments were barely visible (Fig. 1E2).

Meristematic cells treated with the cyanobacterial extract (Fig. 2) also exhibited disoriented cortical actin filaments after 30 min of exposure (Fig. 2A2), as well as bundling effects (indicative arrowheads in Figs 2B1, B2, C1, C2) after 1 and 2 h. After 24 h, apart from F-actin bundling (arrowhead in Fig. 2D2), several cells appeared totally devoid of actin filaments (star in Fig. 2D1).

In the differentiation zone, F-actin cables could be observed in untreated cells, exhibiting a predominant longitudinal orientation (Fig. 3A). After treatment with MC-LR, disorientation and bundling of F-actin was detectable (arrowheads in Figs 3B-E) between 30 min and 2 h of exposure, eventually leading to disappearance of F-actin in large areas of the tissue after 24 h (Fig. 3E).

In roots treated with the extract (Fig. 4), F-actin bundles were disoriented, an effect increasing in a time-dependent manner (arrows in Figs 4A, B, C1, D1). Furthermore, F-actin rings occurred in the affected cells after longer exposure (Figs 4C2, D2, D3). After 24 h, several cells were devoid of F-actin (Fig. 4D1).

CTCF measurements (Fig. 5) confirmed the hypothesis that fluorescence intensity gradually diminishes during the treatment with either MC-LR or the extract, in both meristematic and elongation zone the lowest levels being recorded after 24 h of treatment. This decrease appeared to be especially steep in MC-LR treated roots,

bioRxiv preprint doi: https://doi.org/10.1101/2020.02.17.952218; this version posted February 18, 2020. The copyright holder for this preprint (which was not certified by peer review) is the author/funder, who has granted bioRxiv a license to display the preprint in perpetuity. It is made available under aCC-BY-NC-ND 4.0 International license.

278 just after 30 min of treatment. Any temporary increases in fluorescence intensity (e.g.
279 in differentiated root cells after 1 h of treatment with the extract) could be attributed to
280 F-actin bundling effects.
281
282 **Effects on microtubules and chromatin**
283 Untreated meristematic root cells exhibited the typical microtubule arrays, i.e. cortical
284 microtubules in interphase cells (Fig. S1A), the preprophase band and perinuclear
285 microtubules in preprophase/prophase cells (Fig. S1B), the mitotic spindle in
286 metaphase/anaphase cells (Fig. S1C) and the phragmoplast in telophase/cytokinetic
287 cells (Fig. S1D).
288 Rice root cells treated with the toxic cyanobacterial extract for 30 min-24 h exhibited
289 various time-dependent alterations in the organization of microtubules (Fig. S1E-K).
290 After 30 min of exposure, cortical microtubules of interphase cells were significantly
291 fewer (Fig. S1E; *cf*. S1A). In affected preprophase cells, preprophase bands were
292 visible, but perinuclear microtubules were absent (Fig. S1F; *cf*. S1B). In affected cells
293 with condensed chromosomes, as assessed by DAPI staining, typical spindles were
294 not found, as microtubules connected to the chromosomes appeared either
295 abnormally elongated (Fig. S1G) or short and disoriented (Fig. S1H). In the above
296 affected mitotic cells, microtubule fragments and/or fluorescent tubulin structures,
297 apart from chromosome-connected microtubules, could also be observed (Figs S1G,
298 H). In telophase/cytokinetic cells treated as above, phragmoplasts could be
299 observed, the microtubules of which were longer than those of untreated cells (Fig.
300 S1I; *cf*. S1D), their (-) ends sometimes attached on the surface of daughter nuclei.
301 After 1 h of treatment, microtubules were depolymerized (Figs S1J, K) in cells with
302 normal-looking nucleus (Fig. S1J), as well as in cells with abnormal chromatin
303 condensation (Fig. S1K). In some of these cells, fluorescent tubulin spots could be
304 observed (Fig. S1J).

bioRxiv preprint doi: https://doi.org/10.1101/2020.02.17.952218; this version posted February 18, 2020. The copyright holder for this preprint (which was not certified by peer review) is the author/funder, who has granted bioRxiv a license to display the preprint in perpetuity. It is made available under aCC-BY-NC-ND 4.0 International license.

Interestingly, MC-LR-treated root cells exhibited control-like microtubule arrays. Occasionally, 30 min- and 1 h-treated interphase cells with typical cortical microtubules (Figs S2C, E; *cf.* S2A) exhibited endoplasmic microtubules, not typically observed in untreated cells (Figs S2D, F; *cf.* S2B), while in affected preprophase cells preprophase bands exhibited gaps (Fig S2G; *cf.* Fig. S2H). MC-LR-affected metaphase cells appeared to have typical mitotic spindles (Figs S2I, J; *cf.* Fig. S1C), while occasionally chromosomes out of the spindle could be observed (arrow in Fig. S2J).

Effects on cell cycle progression

The assessment of cell cycle stages in treated root tip cells revealed that each stage frequency was significantly altered after 1 h of treatment with MC-LR, while it was severely disturbed in extract-treated roots even after 30 min (Table 1). In the latter case, the percentage of preprophase/prophase cells was increased after 30 min of treatment, as was the percentage of metaphase/anaphase cells after 1 h, compared to untreated roots. On the contrary, there was a notable decrease in the percentage of cytokinetic cells after 30 min and 1 h of treatment with the extract. Alterations observed (in both MC-LR- and extract-treated roots) were statistically significant (chi-squared test, df = 3, P <0.001)

Effects on cytoplasmic streaming

Alterations of cytoplasmic streaming in affected root cells were visible after treatment with the extract (see Supplementary Videos). After 1 h, streaming either stopped or appeared to be slower (left and right arrow, respectively, Video S5; *cf.* S4), as opposed to that of root cells in presence of water, in which streaming remained vivid during the exposure time period (Videos S1-3). After 2 h, streaming (where present) was noticeably abnormal and cytoplasmic aggregates could be observed (arrow and arrowhead, respectively, Video S6; *cf.* S4).

bioRxiv preprint doi: https://doi.org/10.1101/2020.02.17.952218; this version posted February 18, 2020. The copyright holder for this preprint (which was not certified by peer review) is the author/funder, who has granted bioRxiv a license to display the preprint in perpetuity. It is made available under aCC-BY-NC-ND 4.0 International license.

Effects on the endoplasmic reticulum and Golgi apparatus

The toxic extract also affected the integrity and distribution of the endoplasmic reticulum. In cells exposed to the extract for 30 min and 1 h, fluorescent endoplasmic reticulum aggregates were observed by CLSM, located cortically and/or around the nucleus (Fig. 6B, C), in contrast to the evenly distributed endoplasmic reticulum of untreated cells (Fig. 6A). After 3 h of treatment, these aggregates appeared to fade, while the nucleus exhibited morphological alteration (Fig. 6D).

TEM observations of root cells treated with the extract for 30 min revealed that endoplasmic reticulum cisternae were heavily stacked (Fig. 6F), in contrast to the loosely packed cisternae of untreated cells (Fig. 6E). In addition, while in untreated cells Golgi dictyosomes were evenly distributed (Fig. 7A), in cells affected by the extract the dictyosomes appeared clustered, even after 30 min of treatment with vesicles trapped among them (Fig. 7B). After 1 h of exposure, Golgi apparatus clustering and vesicle aggregation were intensified (Fig. 7C).

DISCUSSION

In this study, MC-LR disrupted F-actin in rice roots. The detrimental effects were recorded as significant alterations of the network (Figs 1, 3) and as a gradual decrease in F-actin fluorescence intensity (Fig. 5), eventually leading to a collapse in both meristematic and differentiating root cells (Figs 1, 3).

Apart from the above similarity, there was a significant difference between the treatment with purified MC-LR and the extract. Exposure to the latter induced severe disruption of microtubule arrays and alterations of the frequency of cells at various cell cycle stages after just 30 min (Table 1). On the contrary, MC-LR affected microtubule organization only slightly, as well as cell cycle distribution only after 1 h of exposure.

bioRxiv preprint doi: https://doi.org/10.1101/2020.02.17.952218; this version posted February 18, 2020. The copyright holder for this preprint (which was not certified by peer review) is the author/funder, who has granted bioRxiv a license to display the preprint in perpetuity. It is made available under aCC-BY-NC-ND 4.0 International license.

360 According to cytological studies on other plant species, MCs affect the integrity and
361 organization of microtubules, causing chromatin hypercondensation in plant cells by
362 inhibiting PP1 and PP2A, which subsequently leads to histone H3
363 hyperphosphorylation (Beyer et al., 2012; Máthé et al., 2009; Ujvárosi et al., 2019).
364 Also, experiments on *Arabidopsis thaliana* indicated the involvement of subfamily II
365 and TON2 subunits of the PP2A holoenzyme in cortical microtubule organization
366 and, probably, in microtubule nucleation through interaction with γTuRCs (Yoon et
367 al., 2018). Studies on PP2A have highlighted its importance for plant cytoskeleton
368 organization (especially microtubules), affecting preprophase band formation,
369 division plane determination (Spinner et al., 2013), and cell shape (Kirik et al., 2012).
370 Interestingly, in the present study, treatment with purified MC-LR did not result in any
371 of these effects. A possible reason for this could be that the duration of treatments
372 here was far shorter than in the previously mentioned studies. In most of the relevant
373 studies, exposure to MC-LR spanned from 4 h to 20 days (Beyer et al., 2012; Garda
374 et al., 2016; Mathé et al., 2009). However, in the present study microtubules were
375 severely affected only after treatment with the crude toxic extract for a very short time
376 (30 min and 1 h), which indicates the possible involvement of other compounds in the
377 effect mechanism. Except of microcystins, which have been detected in *Microcystis*
378 *flos-aquae* TAU-MAC 1510, it is also likely that these effects may be the result of a
379 synergistic action of various bioactive compounds produced by the strain. For
380 example, anabaenopeptins, which show activity against PP1 (Gkelis et al., 2006), are
381 known to occur in large concentrations in *Microcystis*-dominated blooms (Gkelis et
382 al., 2015b) or microginins, which have been recently reported to be abundant in
383 blooms of Greek freshwater cyanobacteria (Zervou et al., 2020), are also known to
384 be bioactive (Ujvárosi et al., 2020; for a review on the variety of cyanobacterial
385 bioactive compounds, see Dittmann et al., 2015; Elisabeth & Janssen, 2019).
386 The findings of the present study prove that F-actin is indeed a target of
387 cyanobacterial toxicity, specifically of microcystins, in plant cells. To date, information

bioRxiv preprint doi: https://doi.org/10.1101/2020.02.17.952218; this version posted February 18, 2020. The copyright holder for this preprint (which was not certified by peer review) is the author/funder, who has granted bioRxiv a license to display the preprint in perpetuity. It is made available under aCC-BY-NC-ND 4.0 International license.

388 about the way actin filaments are affected by microcystins derives exclusively from
389 studies on treated animal cells. In rat hepatocytes and fibroblasts, all three
390 cytoskeletal components (microtubules, intermediate filaments and microfilaments)
391 are sensitive to MC-LR treatments in a dose- and time-dependent manner
392 (Wickstrom et al., 1995). Disorganization of intermediate filaments and microtubules
393 was reported to precede alterations in normal disposition of microfilaments in animal
394 cells. These alterations included extensive reorganization of F-actin into “rosette-like
395 structures”, which eventually collapsed, forming aggregates around the cell nucleus
396 (Wickstrom et al. 1995). Similar observations concerning F-actin were also made in
397 rat hepatocytes by Ghosh et al. (1995) and by Batista et al. (2003) in primary human
398 hepatocytes, while Gácsi et al. (2009) reported the formation of circular actin
399 aggregations around the nuclei of MC-LR-treated Chinese hamster ovary (CHO-K1)
400 cells after 24 h of incubation at high concentrations of the cyanotoxin (20 μM). In
401 particular, actin aggregation at the cell periphery seems to be a common alteration in
402 microcystin-treated animal cells (Eriksson et al., 1989; Falconer and Yeung, 1992;
403 Runnegar and Falconer, 1986; Wickstrom et al., 1995), at least for some time during
404 the cascade of F-actin-collapse events. As expected, alterations in F-actin
405 organization consequently led to animal cell shape deformation.
406 It could be suggested that F-actin disruption in rice root cells is attributed to protein
407 phosphatase inhibition. In human T lymphocytes, inhibition of PP1 and PP2A has
408 been shown to block dephosphorylation of actin depolymerizing factor (ADF)/cofilin,
409 an actin-binding protein, which is responsible for actin depolymerization when in
410 active, unphosphorylated state (Ambach et al., 2000). Such an effect on PP1 and
411 PP2A could explain the bundling effects observed in the F-actin network of rice root
412 cells affected by microcystin, as F-actin tends to become stabilized. In a more recent
413 study (Wang et al., 2014), MC-LR was found to directly bind to PP2A in SMMC-7721
414 human liver cancer cells, inhibiting enzyme activity and causing cytoskeletal
415 rearrangements. More specifically, PP2A inhibition led to hyperphosphorylation of

bioRxiv preprint doi: https://doi.org/10.1101/2020.02.17.952218; this version posted February 18, 2020. The copyright holder for this preprint (which was not certified by peer review) is the author/funder, who has granted bioRxiv a license to display the preprint in perpetuity. It is made available under aCC-BY-NC-ND 4.0 International license.

various cytoskeleton-associated proteins (including cofilins) and inactivation (as well as changes in subcellular localization) of Rac1, a small GTPase, which is regulated by PP2A (Nunbhakdi-Craig et al., 2003) and is involved in microtubule and actin dynamics (Wittmann et al., 2003). In plants, the presence of cofilins has been reported in various species (Hussey et al., 2002), while PP2A-2, an isoform of PP2A, is known to directly regulate ADF/cofilin (and, therefore, F-actin rearrangements) in *Arabidopsis thaliana* (Wen et al., 2012). In addition, OsRac1 (a rice homolog of Rac1), along with its activator GEF protein OsSPK1, have been recently suggested to be regulators of actin dynamics in rice (Wang et al., 2018).

Importantly, in rice root cells, progression of F-actin disorganization/disorientation appeared to be slower than in animal cells and not as harsh; in fact, even after 24 h of exposure, actin filaments could still be observed, though scarce. The increased resistance of actin filaments to microcystins could be attributed to at least three reasons: (1) Most of the actin filaments, especially in vacuolated cells, are interconnected in thick bundles, which could offer stabilization against adverse factors. (2) Cortical actin filaments are interconnected to cellulose microfibrils of the cell wall by formin1 (Martinière et al., 2011), also regulating F-actin stability and cell shape (Rosero et al. 2013, 2016). (3) F-actin may appear more stabilized following inactivation of ADF/cofilin, due to inhibition of protein phosphatases by microcystins.

Whichever the mechanism by which F-actin is affected by microcystins, the effect of a microcystin-rich crude extract indicates that this could occur in environmental conditions, due to cell lysis during cyanobacterial blooms. According to this view, disruption of F-actin may be one more possible reason for cyanobacterial toxicity to plants, apart from the already established effects on microtubules and the cell cycle.

In addition, the importance of F-actin disorganization is also reflected on the alterations observed in endoplasmic reticulum and the Golgi apparatus. As reviewed by Volkmann and Baluška (1999), movement and distribution of endoplasmic reticulum and the Golgi apparatus in plant cells are controlled by the F-actin network.

bioRxiv preprint doi: https://doi.org/10.1101/2020.02.17.952218; this version posted February 18, 2020. The copyright holder for this preprint (which was not certified by peer review) is the author/funder, who has granted bioRxiv a license to display the preprint in perpetuity. It is made available under aCC-BY-NC-ND 4.0 International license.

Furthermore, cytoplasmic streaming was disturbed (see Supplementary Videos), due to its dependence on actomyosin integrity and function (for a review, see Shimmen and Yokota, 2004). Consequently, stacking of endoplasmic reticulum as well as abnormal aggregation of Golgi dictyosomes could be a direct result of defective F-actin organization and subsequent intracellular motility defects. Apart from the involvement of F-actin, alterations of endoplasmic reticulum have been reported in both plant (Huang et al., 2009) and animal cells, either fish (Li et al., 2001) or mammalian (Alverca et al., 2009), and attributed to microcystins, after treatment for various time periods, ranging from hours to days. These results, therefore, suggest the presence of a mechanism of toxicity, which involves microcystins and affects a variety of cell systems. Nevertheless, in the present study, endoplasmic reticulum cisternae seemed to diminish after 1 h of exposure. Interestingly, absence of smooth endoplasmic reticulum has been also previously observed in rat hepatocytes after treatment with MC-LR for 20 min (Eriksson et al., 1989).

In conclusion, F-actin is a target of MC-LR. In addition, the microcystin-rich extract of the cyanobacterial strain *Microcystis flos-aquae* TAU-MAC 1510 disrupts cytoskeletal components, F-actin and microtubules, as well as the endomembrane system and cell cycle distribution, in root tip cells of *Oryza sativa*. Microcystins present in the extract could be held responsible for certain of the effects observed, as they have previously been linked with defects in chromatin condensation, but most probably a synergistic action of microcystins with other cyanobacterial bioactive compounds may be hypothesized. To our best knowledge, this is the first report of a microcystin (MC-LR) affecting the plant F-actin cytoskeleton and the first attempt to feature the potent effects of cyanobacterial bioactive compounds on F-actin-related cell functions. Further research is needed in order to elucidate the above in detail.

ACKNOWLEDGEMENTS

bioRxiv preprint doi: https://doi.org/10.1101/2020.02.17.952218; this version posted February 18, 2020. The copyright holder for this preprint (which was not certified by peer review) is the author/funder, who has granted bioRxiv a license to display the preprint in perpetuity. It is made available under aCC-BY-NC-ND 4.0 International license.

This research is part of a PhD thesis (Dimitris Pappas) and is co-financed by Greece and the European Union (European Social Fund- ESF) through the Operational Programme «Human Resources Development, Education and Lifelong Learning» in the context of the project “Strengthening Human Resources Research Potential via Doctorate Research” (MIS-5000432), implemented by the State Scholarships Foundation (ΙΚΥ). Emmanuel Panteris is supported by the AUTh Research Committee (Grant No 91913). The authors would like to deeply thank Prof. Kaarina Sivonen (University of Helsinki, Finland) for generously providing a stock of MC-LR, as well as Assist. Prof. Ioannis-Dimosthenis Adamakis (National and Kapodistrian University of Athens, Greece) and Assoc. Prof. George Komis (Palacký University Olomouc, Czechia) for their advice and critical reading of the manuscript.

REFERENCES

Adamakis I.-D.S., Panteris E., Eleftheriou E.P. (2014) The nitrate reductase inhibitor, tungsten, disrupts actin microfilaments in *Zea mays* L. *Protoplasma*, **251**, 567-574.

Adamakis I.-D.S., Panteris E., Eleftheriou E.P. (2016) Bisphenol A disrupts microtubules and induces multipolar spindles in dividing root tip cells of the gymnosperm *Abies cephalonica*. *Chemosphere*, **149**, 202-210.

Alverca E., Andrade M., Dias E., Sam Bento F., Batoréu M.C.C., Jordan P., Silva M.J., Pereira P. (2009) Morphological and ultrastructural effects of microcystin-LR from *Microcystis aeruginosa* extract on a kidney cell line. *Toxicon*, **54**, 283-294.

Ambach A., Saunus J., Konstandin M., Wesselborg S., Meuer S.C., Samstag Y. (2000) The serine phosphatases PP1 and PP2A associate with and activate the actin-binding protein cofilin in human T lymphocytes. *European Journal of Immunology*, **30**, 3422-3431.

bioRxiv preprint doi: https://doi.org/10.1101/2020.02.17.952218; this version posted February 18, 2020. The copyright holder for this preprint (which was not certified by peer review) is the author/funder, who has granted bioRxiv a license to display the preprint in perpetuity. It is made available under aCC-BY-NC-ND 4.0 International license.

496 Azevedo C.C., Azevedo J., Osório H., Vasconcelos V., Campos A. (2014) Early
497 physiological and biochemical responses of rice seedlings to low concentration of
498 microcystin-LR. *Ecotoxicology*, **23**, 107-121.
499 Batista T., de Sousa G., Šuput J.S., Rahmani R., Šuput D. (2003) Microcystin-LR
500 causes the collapse of actin filaments in primary human hepatocytes. *Aquatic*
501 *Toxicology*, **65**, 85-91.
502 Beyer D., Tándor I., Kónya Z., Bátori R., Roszik J., Vereb G., Erdődi F., Vasas G., M-
503 Hamvas M., Jambrovics K., Máthé C. (2012) Microcystin-LR, a protein
504 phosphatase inhibitor, induces alterations in mitotic chromatin and microtubule
505 organization leading to the formation of micronuclei in *Vicia faba*. *Annals of*
506 *Botany*, **110**, 797-808.
507 Boevink P., Oparka K., Santa Cruz S., Martin B., Betteridge A., Hawes C. (1998)
508 Stacks on tracks: the plant Golgi apparatus traffics on an actin/ER network. *Plant*
509 *Journal*, **15**, 441-447.
510 Brautigan D.L., Shenolikar S. (2018) Protein serine/threonine phosphatases: Keys to
511 unlocking regulators and substrates. *Annual Review of Biochemistry*, **87**, 921-964.
512 Buratti M.F., Manganelli M., Vichi S., Stefanelli M., Scardala S., Testai E., Funari E.
513 (2017) Cyanotoxins: producing organisms, occurrence, toxicity, mechanism of
514 action and human health toxicological risk evaluation. *Archives of Toxicology*, **91**,
515 1049-1130.
516 Cao Q., Rediske R.R., Yao L., Xie L. (2018a) Effect of microcystins on root growth,
517 oxidative response, and exudation of rice (*Oryza sativa*). *Ecotoxicology and*
518 *Environmental Safety*, **149**, 143-149.
519 Cao Q., Steinman A.D., Wan X., Xie L. (2018b) Bioaccumulation of microcystin
520 congeners in soil-plant system and human health risk assessment: A field study
521 from Lake Taihu region of China. *Environmental Pollution*, **240**, 44-50.
522 Catherine A., Bernard C., Spoof L., Bruno M. (2017) Microcystins and Nodularins. In:
523 Meriluoto, J., Spoof, L., Codd, G.A. (Eds.), Handbook of Cyanobacterial

bioRxiv preprint doi: https://doi.org/10.1101/2020.02.17.952218; this version posted February 18, 2020. The copyright holder for this preprint (which was not certified by peer review) is the author/funder, who has granted bioRxiv a license to display the preprint in perpetuity. It is made available under aCC-BY-NC-ND 4.0 International license.

524 Monitoring and Cyanotoxin Analysis. John Wiley and Sons, Ltd., Chichester, UK:
525 109-126.
526 Chen J., Han F.X., Wang F., Zhang H., Zhiqi S. (2012) Accumulation and
527 phytotoxicity of microcystin-LR in rice (*Oryza sativa*). *Ecotoxicology and*
528 *Environmental Safety*, **76**, 193-199.
529 Codd G.A., Meriluoto J., Metcalf J.S. (2017) Introduction: Cyanobacteria,
530 Cyanotoxins, Their Human Impact, and Risk Management. In: Meriluoto, J.,
531 Spoof, L., Codd, G.A. (Eds.), Handbook of Cyanobacterial Monitoring and
532 Cyanotoxin Analysis. John Wiley and Sons, Ltd., Chichester, UK: 3-8.
533 Corbel S., Mougin C., Nélieu S., Delarue G., Bouaïcha N. (2016) Evaluation of the
534 transfer and the accumulation of microcystins in tomato (*Solanum lycopersicum*
535 cultivar MicroTom) tissues using a cyanobacterial extract containing microcystins
536 and the radiolabeled microcystin-LR (^{14}C-MC-LR). *Science of the Total*
537 *Environment*, **541**, 1052-1058.
538 Dittmann E., Gugger M., Sivonen K., Fewer D.P. (2015) Natural product biosynthetic
539 diversity and comparative genomics of the cyanobacteria. *Trends in Microbiology*,
540 **23**, 642-652.
541 Drobac D., Tokodi N., Kiprovski B., Malenčić D., Važić T., Nybom S., Meriluoto J.,
542 Svirčev Z. (2017) Microcystin accumulation and potential effects on antioxidant
543 capacity of leaves and fruits of *Capsicum annuum*. *Journal of Toxicology and*
544 *Environmental Health, Part A*, **80**, 145-154.
545 Elisabeth M., Janssen L. (2019) Cyanobacterial peptides beyond microcystins – A
546 review on co-occurrence, toxicity, and challenges for risk assessment. *Water*
547 *Research*, **151**, 488-499.
548 Eriksson J.E., Paatero G.I.L., Meriluoto J.A.O., Codd G.A., Kass G.E.N., Nicotera P.,
549 Orrenius S. (1989) Rapid microfilament reorganization induced in isolates rat
550 hepatocytes by microcystin-LR, a cyclic peptide toxin. *Experimental Cell*
551 *Research*, **185**, 86-100.

bioRxiv preprint doi: https://doi.org/10.1101/2020.02.17.952218; this version posted February 18, 2020. The copyright holder for this preprint (which was not certified by peer review) is the author/funder, who has granted bioRxiv a license to display the preprint in perpetuity. It is made available under aCC-BY-NC-ND 4.0 International license.

552 Falconer I.R., Yeung D.S.K. (1992) Cytoskeletal changes in hepatocytes induced by
553 *Microcystis* toxins and their relation to hyperphosphorylation of cell proteins.
554 *Chemico-Biological Interactions*, **81**, 181-196.
555 FAO Rice Market Monitor (2018) Volume XXI, Issue No. 1.
556 Gácsi M., Antal O., Vasas G., Máthé C., Borbély G., Saker M.L., Győri J., Farkas A.,
557 Vehovszky Á., Bánfalvi G. (2009) Comparative study of cyanotoxins affecting
558 cytoskeletal and chromatin structures in CHO-K1 cells. *Toxicology in Vitro*, **23**,
559 710-718.
560 Garda T., Kónya Z., Tándor I., Beyer D., Vasas G., Erdődi F., Vereb G., Papp G.,
561 Riba M., M-Hamvas M., Máthé C. (2016) Microcystin-LR induces mitotic spindle
562 assembly disorders in *Vicia faba* by protein phosphatase inhibition and not
563 reactive oxygen species induction. *Journal of Plant Physiology*, **199**, 1-11.
564 Gavet O., Pines J. (2010) Activation of cyclin B1-Cdk1 synchronizes events in the
565 nucleus and the cytoplasm at mitosis. *Journal of Cell Biology*, **189**, 247-259.
566 Ghosh S., Khan S.A., Wickstrom M., Beasley V. (1995) Effects of microcystin-LR on
567 actin and the actin-associated proteins α-actinin and talin in hepatocytes. *Natural*
568 *Toxins*, **3**, 405-414.
569 Gkelis S., Lanaras T., Sivonen K. (2006) The presence of microcystins and other
570 cyanobacterial bioactive peptides in aquatic fauna collected from Greek lakes.
571 *Aquatic Toxicology*, **78**, 32-41.
572 Gkelis S., Lanaras T., Sivonen K. (2015b) Cyanobacterial toxic and bioactive
573 peptides in freshwater bodies of Greece: concentrations, occurrence patterns and
574 implications for human health. *Marine Drugs*, **13**, 6319-6335.
575 Gkelis S., Panou M. (2016) Capturing biodiversity: linking a cyanobacteria culture
576 collection to the “scratchpads” virtual research environment enhances biodiversity
577 knowledge. *Biodiversity Data Journal*, **4**: e7965.
578 Gkelis S., Panou M., Konstantinou D., Apostolidis P., Kasampali A., Papadimitriou S.,
579 Kati D., Di Lorenzo G.M., Ioakeim S., Zervou S.-K., Christophoridis C., Triantis

bioRxiv preprint doi: https://doi.org/10.1101/2020.02.17.952218; this version posted February 18, 2020. The copyright holder for this preprint (which was not certified by peer review) is the author/funder, who has granted bioRxiv a license to display the preprint in perpetuity. It is made available under aCC-BY-NC-ND 4.0 International license.

580 T.M., Kaloudis T., Hiskia A., Arsenakis M. (2019) Diversity, cyanotoxin production,
581 and bioactivities of cyanobacteria isolated from freshwaters of Greece. *Toxins*, **11**,
582 436.
583 Gkelis S., Tussy P.F., Zaoutsos N. (2015a) Isolation and preliminary characterization
584 of cyanobacteria strains from freshwaters of Greece. *Open Life Sciences*, **10**, 52-
585 60.
586 Haalinen K., Jokela, J., Fewer D.P., Wahlsten M., Sivonen K. (2007) Direct evidence
587 for production of microcystins by *Anabaena* strains from the Baltic Sea. *Applied*
588 *and Environmental Microbiology*, **73**, 6543-6550.
589 Huang W., Xing W., Li D., Liu Y. (2009) Morphological and ultrastructural changes in
590 tobacco BY-2 cells exposed to microcystin-RR. *Chemosphere*, **76**, 1006-1012.
591 Hussey P.J., Allwood E.G., Smertenko A.P. (2002) Actin-binding proteins in the
592 *Arabidopsis* genome database: properties of functionally distinct plant actin-
593 depolymerizing factors/cofilins. *Philosophical Transactions of the Royal Society B*,
594 **357**, 791-798.
595 Kirik A., Ehrhardt D.W., Kirik V. (2012) *TONNEAU2/FASS* regulates the geometry of
596 microtubule nucleation and cortical array organization in interphase *Arabidopsis*
597 cells. *Plant Cell*, **24**, 1158-1170.
598 Li X., Liu Y., Song L. (2001) Cytological alterations in isolated hepatocytes from
599 common carp (*Cyprinus carpio* L.) exposed to microcystin-LR. *Environmental*
600 *Toxicology*, 16, 517-522.
601 Liang C., Wang W., Wang Y. (2016) Effect of irrigation with microcystins-
602 contaminated water on growth, yield and grain quality of rice (*Oryza sativa*).
603 *Environmental Earth Sciences*, **75**, 505-514.
604 MacKintosh C., Beattie K.A., Klumpp S., Cohen P., Codd G.A. (1990) Cyanobacterial
605 microcystin-LR is a potent and specific inhibitor of protein phosphatases 1 and 2A
606 from both mammals and higher plants. *FEBS Letters*, **264**, 187-192.

bioRxiv preprint doi: https://doi.org/10.1101/2020.02.17.952218; this version posted February 18, 2020. The copyright holder for this preprint (which was not certified by peer review) is the author/funder, who has granted bioRxiv a license to display the preprint in perpetuity. It is made available under aCC-BY-NC-ND 4.0 International license.

607 Martinière A., Gayral P., Hawes C., Runions J. (2011) Buliding bridges: formin1 of
608 Arabidopsis forms a connection between the cell wall and the actin cytoskeleton.
609 *Plant Journal*, **66**, 354-365.
610 Máthé C., Beyer D., Erdődi F., Serfőző Z., Székvölgyi L., Vasas G., M-Hamvas M.,
611 Jámbrik K., Gonda S., Kiss A., Szigeti Z.M., Surányi G. (2009) Microcystin-LR
612 induces abnormal root development by altering microtubule organization in tissue-
613 cultured common reed (*Phragmites australis*) plantlets. *Aquatic Toxicology*, **92**,
614 122-130.
615 Máthé C., M-Hamvas M., Vasas G. (2013) Microcystin-LR and cylindrospermopsin
616 induced alterations in chromatin organization of plant cells. *Marine Drugs*, **11**,
617 3689-3717.
618 Mitrovic S.M., Pflugmacher S., James K.J., Furey A. (2004) Anatoxin-a elicits an
619 increase in peroxidase and glutathione S-transferase activity in aquatic plants.
620 *Aquatic Toxicology*, **68**, 185-192.
621 Mylona Z., Panteris E., Kevrekidis T., Malea P. (2020) Silver nanoparticle toxicity
622 effect on the seagrass *Halophila stipulacea*. *Ecotoxicology and Environmental*
623 *Safety*, **189**, 109925.
624 Nunbhakdi-Craig V., Craig L., Machleidt T., Sontag E. (2003) Simian virus 40 small
625 tumor antigen induces deregulation of the actin cytoskeleton and tight junctions in
626 kidney epithelial cells. *Journal of Virology*, **77**, 2807-2818.
627 Pantelić D., Svirčev Z., Simeunović J., Vidović M., Trajković I. (2013) Cyanotoxins:
628 Characteristics, production and degradation routes in drinking water treatment
629 with reference to the situation in Serbia. *Chemosphere*, **91**, 421-441.
630 Pflugmacher S., Aulhorn M., Grimm B. (2007) Influence of a cyanobacterial crude
631 extract containing microcystin-LR on the physiology and antioxidative defence
632 systems of different spinach variants. *New Phytologist*, **175**, 482-489.
633 Prieto A., Campos A., Cameán A., Vasconcelos V. (2011) Effects on growth and
634 oxidative stress status of rice plants (*Oryza sativa*) exposed to two extracts of

bioRxiv preprint doi: https://doi.org/10.1101/2020.02.17.952218; this version posted February 18, 2020. The copyright holder for this preprint (which was not certified by peer review) is the author/funder, who has granted bioRxiv a license to display the preprint in perpetuity. It is made available under aCC-BY-NC-ND 4.0 International license.

toxin-producing cyanobacteria (*Aphanizomenon ovalisporum* and *Microcystis aeruginosa*). *Ecotoxicology and Environmental Safety*, **74**, 1973-1980.

Rippka R. (1988) Isolation and purification of cyanobacteria. *Methods in Enzymology*, **167**, 3-27.

Rosero A., Oulehlová D., Stillerová L., Schiebertová P., Grunt M., Žárský V., Cvrčková F. (2016) Arabidopsis FH1 formin affects cotyledon pavement cell shape by modulating cytoskeleton dynamics. Plant Cell Physiology, 57, 488–504.

Rosero A., Žárský V., Cvrčková F. (2013) AtFH1 formin mutation affects actin filament and microtubule dynamics in *Arabidopsis thaliana*. *Journal of Experimental Botany*, **64**, 585–597.

Runnegar M.T.C., Falconer I.R. (1986) Effect of toxin from the cyanobacterium *Microcystis aeruginosa* on ultrastructural morphology and actin polymerization in isolated hepatocytes. *Toxicon*, **24**, 109-115.

Shimmen T., Yokota E. (2004) Cytoplasmic streaming in plants. *Current Opinion in Cell Biology*, **16**, 68-72.

Sivonen K., Jones G. (1999) Cyanobacterial Toxins. In: Chorus, I., Bartram, J. (Eds.), Toxic Cyanobacteria in Water: A Guide to their Public Health Consequences, Monitoring and Management. E and FN Spon, London: 41-111.

Spinner L., Gadeyne A., Belcram K., Goussot M., Moison M., Duroc Y., Eeckhout D., De Winne N., Schaefer E., Van De Slijke E., Persiau G., Witters E., Gevaert K., De Jaeger G., Bouchez D., Van Damme D., Pastuglia M. (2013) A protein phosphatase 2A complex spatially controls plant cell division. *Nature Communications*, **4**, 1863.

Stavropoulou K., Adamakis I.-D.S., Panteris E., Arseni E.-M., Eleftheriou E.P. (2018) Disruption of actin filaments in *Zea mays* by bisphenol A depends on their crosstalk with microtubules. *Chemosphere*, **195**, 653-665.

bioRxiv preprint doi: https://doi.org/10.1101/2020.02.17.952218; this version posted February 18, 2020. The copyright holder for this preprint (which was not certified by peer review) is the author/funder, who has granted bioRxiv a license to display the preprint in perpetuity. It is made available under aCC-BY-NC-ND 4.0 International license.

661 Ujvárosi A.Z., Hercog K., Riba M., Gonda S., Filipič M., Vasas G., Žegura B. (2020)
662 The cyanobacterial oligopeptides microginins induce DNA damage in the human
663 hepatocellular carcinoma (HepG2) cell line. *Chemosphere*, **240**, 124880.
664 Ujvárosi A.Z., Riba M., Garda T., Gyémánt G., Vereb G., M-Hamvas M., Vasas G.,
665 Máthé C. (2019) Attack of *Microcystis aeruginosa* bloom on a *Ceratophyllum*
666 *submersum* field: Ecotoxicological measurements in real environment with real
667 microcystins exposure. *Science of the Total Environment*, **662**, 735-745.
668 Volkmann D., Baluška F. (1999) Actin cytoskeleton in plants: From transport
669 networks to signaling networks. *Microscopy Research and Technique*, **47**, 135-
670 154.
671 Wang H., Liu J., Lin S., Wang B., Xing M., Guo Z., Xu L. (2014) MCLR-induced PP2A
672 inhibition and subsequent Rac1 inactivation and hyperphosphorylation of
673 cytoskeleton-associated proteins are involved in cytoskeleton rearrangement in
674 SMMC-7721 human liver cancer cell line. *Chemosphere*, **112**, 141-153.
675 Wang Q., Li Y., Ishikawa K.l., Kosami K., Uno K., Nagawa S., Tan L., Du J.,
676 Shimamoto K., Kawano Y. (2018) Resistance protein Pit interacts with the GEF
677 OsSPK1 to activate OsRac1 and trigger rice immunity. *Proceedings of the*
678 *National Academy of Sciences of the United States of America*, **115**, 1551-1560.
679 Wen F., Wang J., Xing D. (2012) A protein phosphatase 2A catalytic subunit
680 modulates blue light-induced chloroplast avoidance movements through regulating
681 actin cytoskeleton in Arabidopsis. *Plant Cell Physiology*, **53**, 1366-1379.
682 Wickstrom M.L., Khan S.A., Haschek W.M., Wyman J.F., Eriksson J.E., Schaeffer
683 D.J., Beasley V.R. (1995) Alterations in microtubules, intermediate filaments, and
684 microfilaments induced by microcystin-LR in cultured cells. *Toxicologic Pathology*,
685 **23**, 326-337.
686 Wittmann T., Bokoch G.M., Waterman-Storer C.M. (2003) Regulation of leading edge
687 microtubule and actin dynamics downstream of Rac1. *Journal of Cell Biology*, **161**,
688 845-851.

bioRxiv preprint doi: https://doi.org/10.1101/2020.02.17.952218; this version posted February 18, 2020. The copyright holder for this preprint (which was not certified by peer review) is the author/funder, who has granted bioRxiv a license to display the preprint in perpetuity. It is made available under aCC-BY-NC-ND 4.0 International license.

689 Yoon J.-T., Ahn H.-K., Pai H.-S. (2018) The subfamily II catalytic subunits of protein
690 phosphatase 2A (PP2A) are involved in cortical microtubule organization. *Planta*,
691 **248**, 1551-1567.
692 Zervou S.-K., Gkelis S., Kaloudis T., Hiskia A., Mazur-Marzec, H. (2020) New
693 microginins from cyanobacteria of Greek freshwaters. *Chemosphere*, **248**,
694 125961.

695

696 **Tables**

697 **Table 1.** Occurrence of various cell cycle stages in *O. sativa* root tips, either control
698 or after treatment with microcystin-LR (MC-LR) or the *Microcystis flos-aquae* TAU-
699 MAC 1510 extract for 30 min and 1 h. Data represent absolute cell counts
700 (percentages in parentheses). Data exhibiting statistically significant difference
701 compared to the control are noted with asterisks (chi-squared test, df = 3, P <0.001).

		MC-LR		*Microcystis flos-aquae* 1510	
	Control (%)	**30 min (%)**	**1 h (%)***	**30 min (%)***	**1 h (%)***
Interphase	1080 (91.6)	1012 (90.68)	978 (92.44)	895 (89.5)	914 (91.4)
Preprophase/Prophase	44 (3.73)	53 (4.75)	44 (4.16)	79 (7.9)	51 (5.1)
Metaphase/ Anaphase	12 (1.02)	8 (0.72)	7 (0.66)	12 (1.2)	31 (3.1)
Cytokinesis	43 (3.65)	43 (3.85)	29 (2.74)	14 (1.4)	4 (0.4)

702

703

704

705

706 **Figure Legends**

bioRxiv preprint doi: https://doi.org/10.1101/2020.02.17.952218; this version posted February 18, 2020. The copyright holder for this preprint (which was not certified by peer review) is the author/funder, who has granted bioRxiv a license to display the preprint in perpetuity. It is made available under aCC-BY-NC-ND 4.0 International license.

Figure 1. Maximum intensity projections of serial CLSM sections (A1, B1, C1, D1, E1, B3, C3-C5) and single cortical CLSM sections (A2, B2, C2, D2, E2) of *O. sativa* protodermal cells in the root meristematic zone, after F-actin staining. treatment with purified MC-LR and/or. In all images the root tip points towards the bottom of the page. Single cortical sections depict cells from the same root areas as the projections, at higher magnification. Control cells exhibit a well-organized network of abundant fine cortical and endoplasmic actin filaments (**A1**). The dominant orientation of cortical actin filaments is transverse (perpendicular to the root axis, **A2**). Cytokinetic cells with prominent F-actin phragmoplasts are noted by arrows (projections **A1**-**E1**). After treatment with MC-LR, cortical actin filaments appear disoriented at 30 min (indicative arrowheads in **B2**; *cf.* **A2**), tending to form bundles after 1 h (indicative arrowheads in **B2, C2, D2**). Ring-shaped F-actin conformations (actin-rings) are visible in affected cells after 30 min and 1 h of treatment (arrowheads in **B3** and **C3-C5**, enlargements of framed areas in **B1** and **C1**, respectively). After 24 h, F-actin fluorescence intensity is noticeably decreased (**E1**) and the cortical F-actin network barely visible (**E2**). Scale bars: 10 μm.

Figure 2. Maximum intensity projections of serial CLSM cortical sections (A1, B1, C1, D1) and single cortical CLSM sections (A2, B2, C2, D2) of *O. sativa* protodermal cells in the root meristematic zone, after treatment with the *M. flos-aquae* TAU-MAC 1510 extract and F-actin staining. All figures are oriented with the root tip to the bottom of the page. Single cortical sections (**A2**-**D2**) depict cells from the same root areas as the projections (**A1**-**D1**), at higher magnification. After 30 min of treatment with the extract (**A1**), cortical actin filaments appear disoriented (**A2**; *cf.* **Fig. 1A2**), tending to form bundles after 1 h (indicative arrowheads in **B1, B2**). After 2 h, bundling increases (indicative arrowheads in **C1, C2**). After 24 h, the F-actin network has collapsed and cells devoid of actin filaments

bioRxiv preprint doi: https://doi.org/10.1101/2020.02.17.952218; this version posted February 18, 2020. The copyright holder for this preprint (which was not certified by peer review) is the author/funder, who has granted bioRxiv a license to display the preprint in perpetuity. It is made available under aCC-BY-NC-ND 4.0 International license.

(area marked with star in **D1**) can be observed, along with remnants of bundles (arrowhead in **D2**). Scale bars: 10 µm.

Figure 3. Maximum intensity projections of serial CLSM sections of *O. sativa* epidermal cells in the root differentiation zone, after F-actin staining. All figures are oriented with the root rip to the bottom of the page. In control cells, longitudinal subcortical F-actin bundles can be observed (**A**). Cells treated with MC-LR for 30 min exhibit disoriented subcortical F-actin bundles, converging at several cell sites (indicative arrowheads in **B**; *cf.* **A**). This effect is also detectable after 1 and 2 h (arrowheads in **C** and **D**, respectively). After 24 h, F-actin bundles have diminished and only remnants of F-actin bundles (arrowheads in **E**) can be observed. Scale bars: 10 µm.

Figure 4. Maximum intensity projections of serial CLSM sections of *O. sativa* epidermal cells in the root differentiation zone, after treatment with the *M. flos-aquae* TAU-MAC 1510 extract and F-actin staining. All figures are oriented with the root rip to the bottom of the page, except for (**C2**, **D2**) with the root tip to the right. After treatment with the extract for 30 min, subcortical F-actin bundles appear to be disoriented (**A**; *cf.* **Fig. 3A**), tending to form aggregates at 1 h (**B**). After 2 h, actin filaments begin to diminish (**C1**) and F-actin rings can be observed (arrows in **C2**, enlargement of the framed area of **C1**). After 24 h, cells devoid of F-actin can be observed (**D1**), while F-actin rings (arrows in **D2** and **D3**, enlargements of framed areas of **D1**) are abundant in cells that still exhibit actin filaments. Scale bars: 10 µm.

Figure 5. Fluorescence intensity measurements of F-actin in *O. sativa* root cells. Maximum intensity projections of serial CLSM sections of the meristematic and differentiation zones of roots treated with the *M. flos-aquae* TAU-MAC 1510 extract (maroon) or purified MC-LR (green) for various durations (30 min, 1, 2 and 24 h) were compared to similar images of control roots. Fluorescence intensity decreases

bioRxiv preprint doi: https://doi.org/10.1101/2020.02.17.952218; this version posted February 18, 2020. The copyright holder for this preprint (which was not certified by peer review) is the author/funder, who has granted bioRxiv a license to display the preprint in perpetuity. It is made available under aCC-BY-NC-ND 4.0 International license.

759 drastically in a time-dependent manner, especially after treatment with MC-LR.
760 Temporary increases, where visible, could be attributed to F-actin bundling effects.
761 Error bars indicate the standard error. All data shown exhibit statistically significant
762 difference compared to control (ANOVA with Dunnett's test), P <0.001. n = 30.

763 **Figure 6. Endoplasmic reticulum distribution in *O. sativa* root cells.** Various
764 durations of treatment with the *M. flos-aquae* TAU-MAC 1510 extract are indicated
765 on the images. **A**-**D**. Single CLSM central sections, after endoplasmic reticulum
766 immunolabeling (green) and DNA staining with DAPI (pseudocoloration in red).
767 Untreated cells (**A**) exhibit even endoplasmic reticulum distribution during interphase
768 (cells at middle and right), while during metaphase endoplasmic reticulum encages
769 the spindle (left). Treatment with the extract results in appearance of endoplasmic
770 reticulum aggregates (arrows in **B-D**), even after only 30 min (**B**), the fluorescence
771 intensity of which fades as treatment duration increases (**C**, **D**). Scale bars: 5 μm. **E**,
772 **F**. TEM micrographs depicting normal endoplasmic reticulum distribution in control
773 cells (**E**) and a stack of endoplasmic reticulum cisternae (arrow in **F**) after 30 min of
774 treatment. After longer treatment, endoplasmic reticulum cisternae could not be
775 found by TEM. Scale bars: 0.2 μm.

776 **Figure 7. TEM micrographs of Golgi dictyosome distribution in *O. sativa* root**
777 **cells.** Dictyosomes are normally distributed and distanced in an untreated cell (**A**).
778 After 30 min (**B**) and 1 h (**C**) of treatment with the *M. flos-aquae* TAU-MAC 1510
779 extract, dictyosomes gather in clusters, displaying aggregates of vesicles (asterisks)
780 entrapped between them. Scale bars: 0.2 μm (**A**, **B**) and 0.5 μm (**C**).

781

782

783

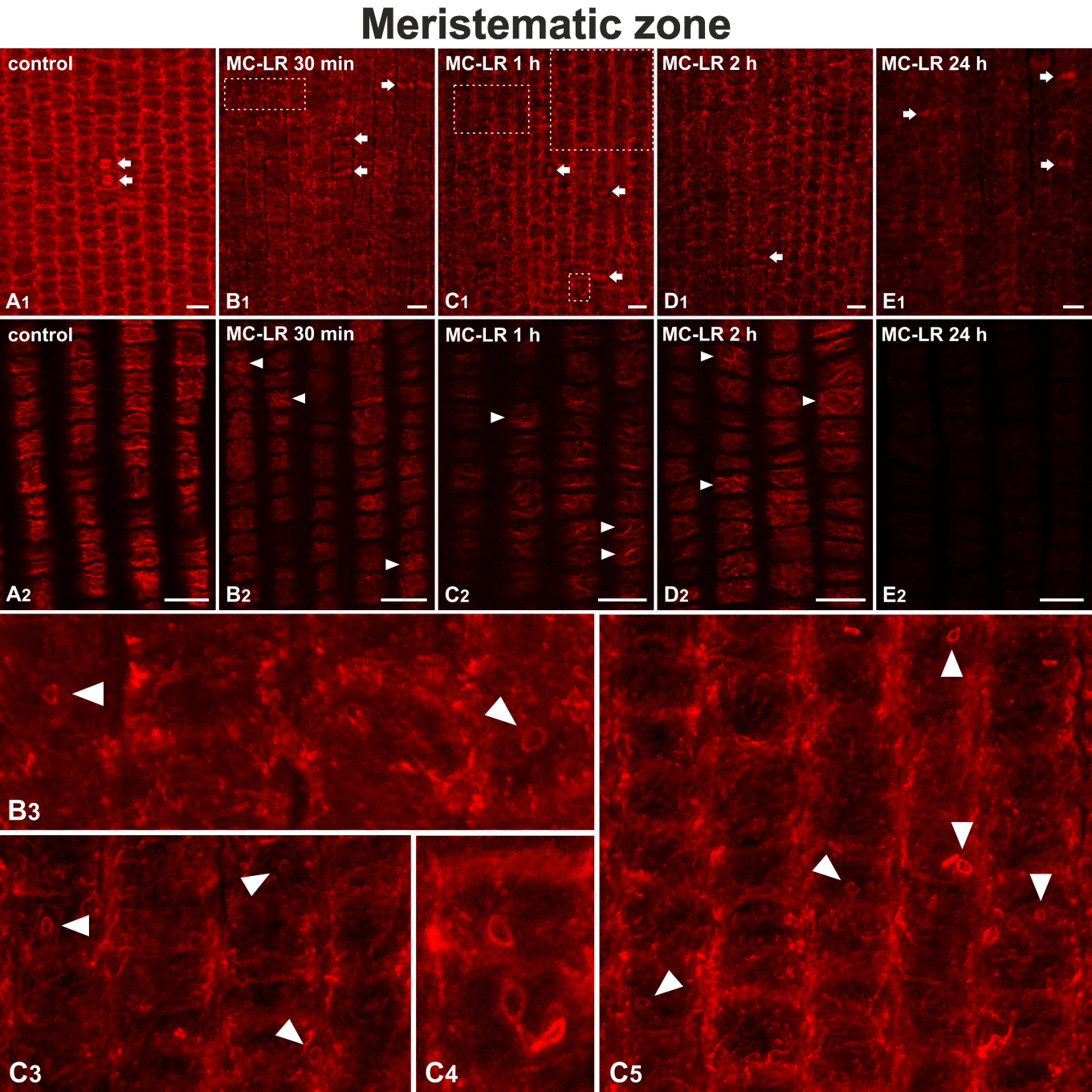
Meristematic zone
control
MC-LR 30 min
MC-LR 1 h
MC-LR 2 h
MC-LR 24 h
A1
B1
C1
D1
E1
control
MC-LR 30 min
MC-LR 1 h
MC-LR 2 h
MC-LR 24 h
A2
B2
C2
D2
E2
B3
C3
C4
C5

Meristematic zone

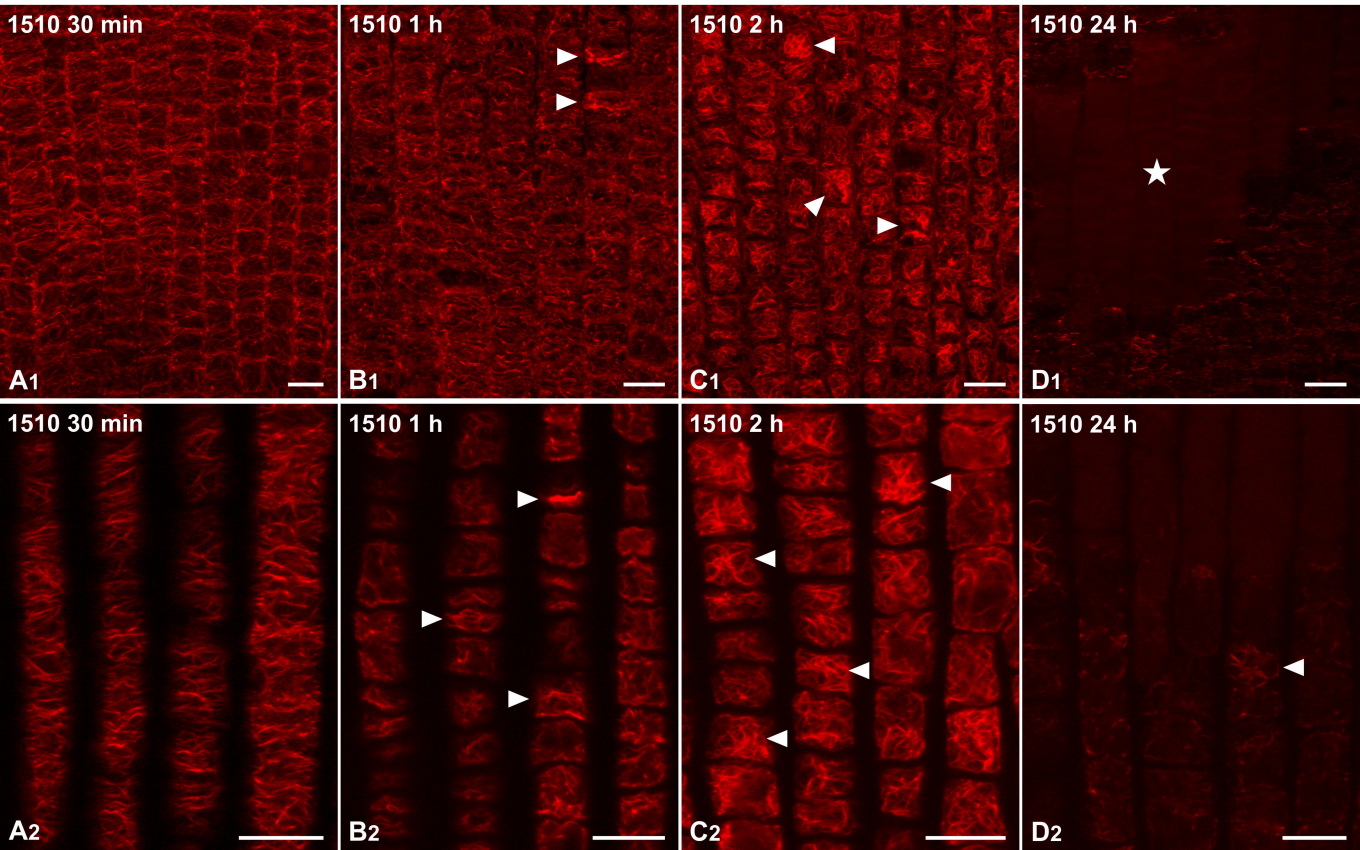

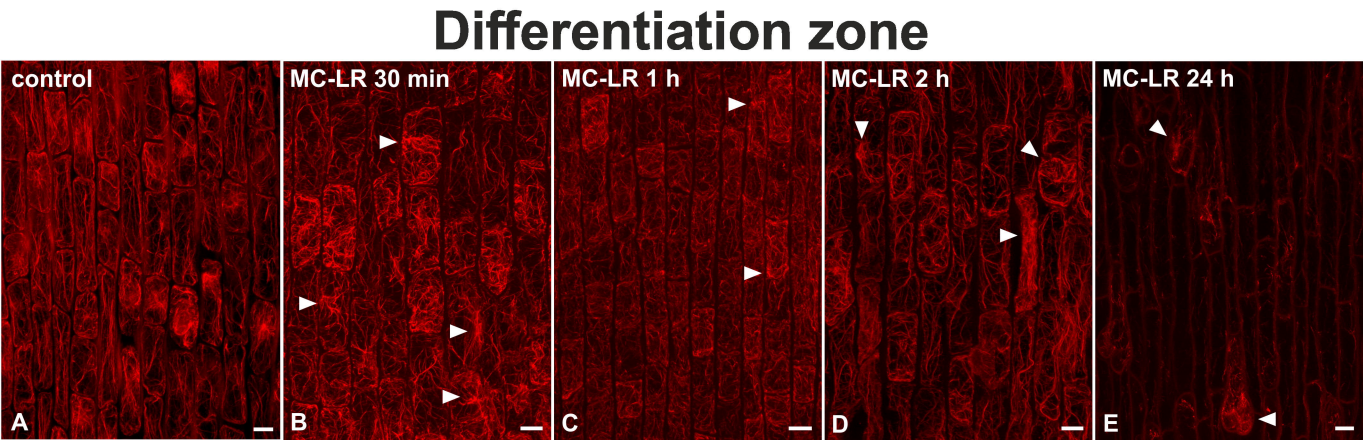
Differentiation zone
control
MC-LR 30 min
MC-LR 1 h
MC-LR 2 h
MC-LR 24 h
A
B
C
D
E

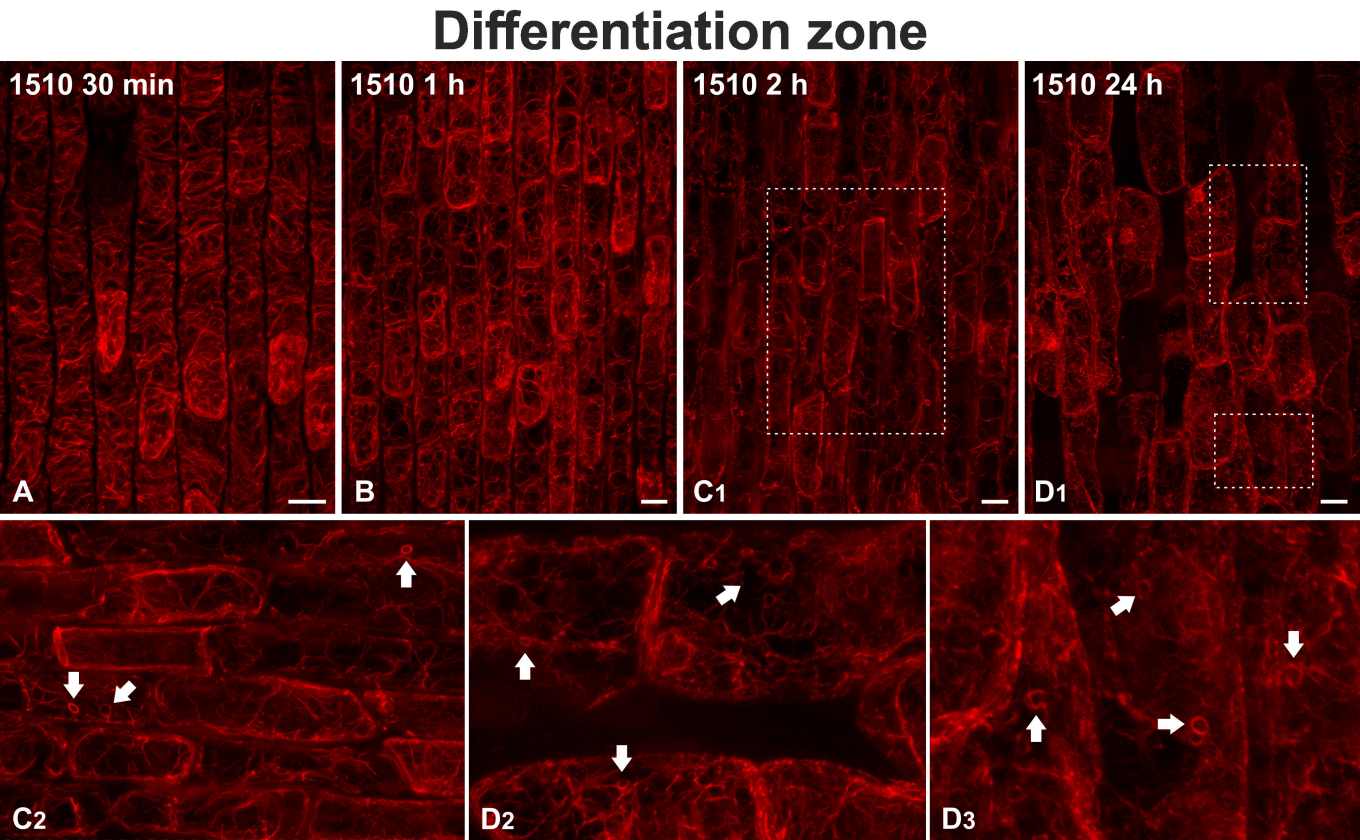
Differentiation zone
1510 30 min
1510 1 h
1510 2 h
1510 24 h
A
B
C1
D1
C2
D2
D3

Meristematic zone

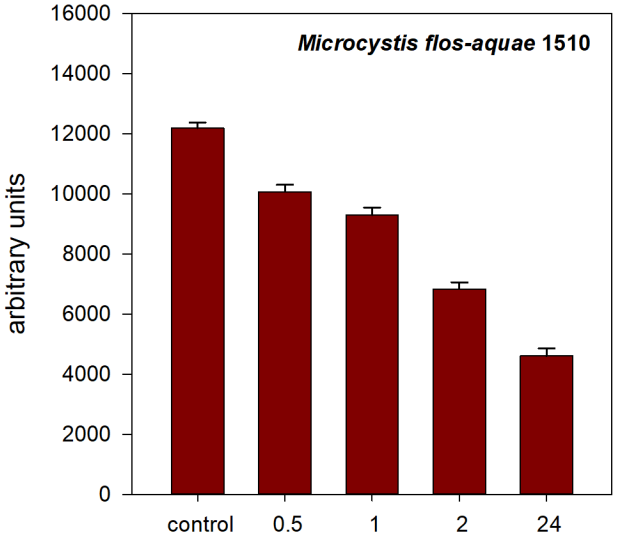

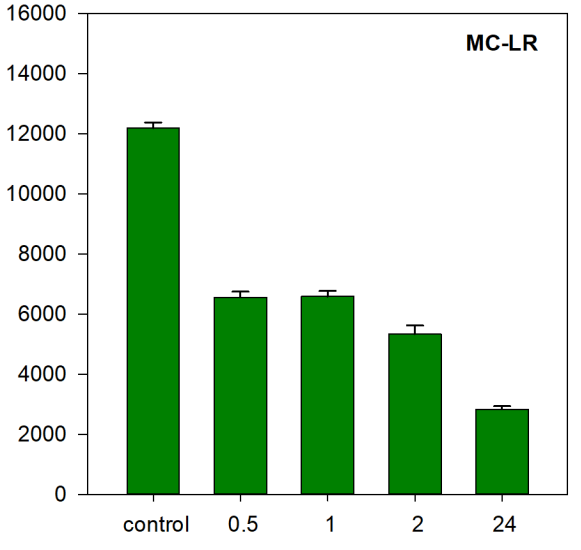

Elongation zone

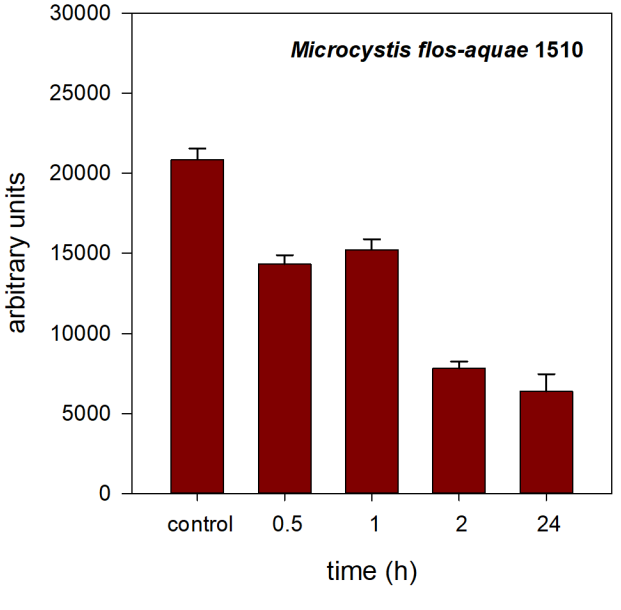

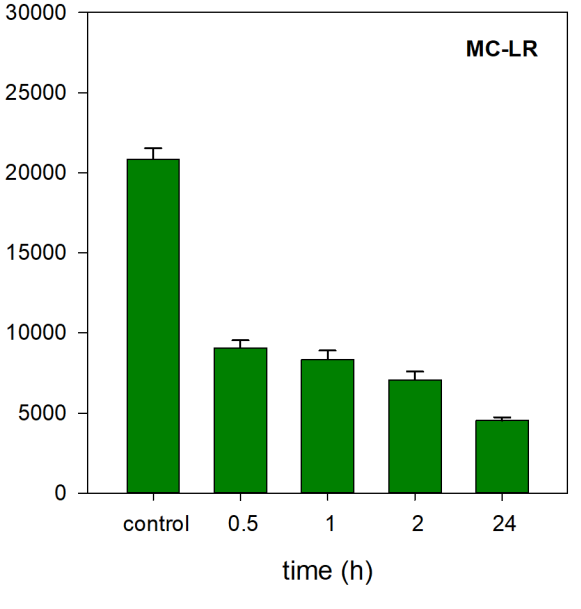

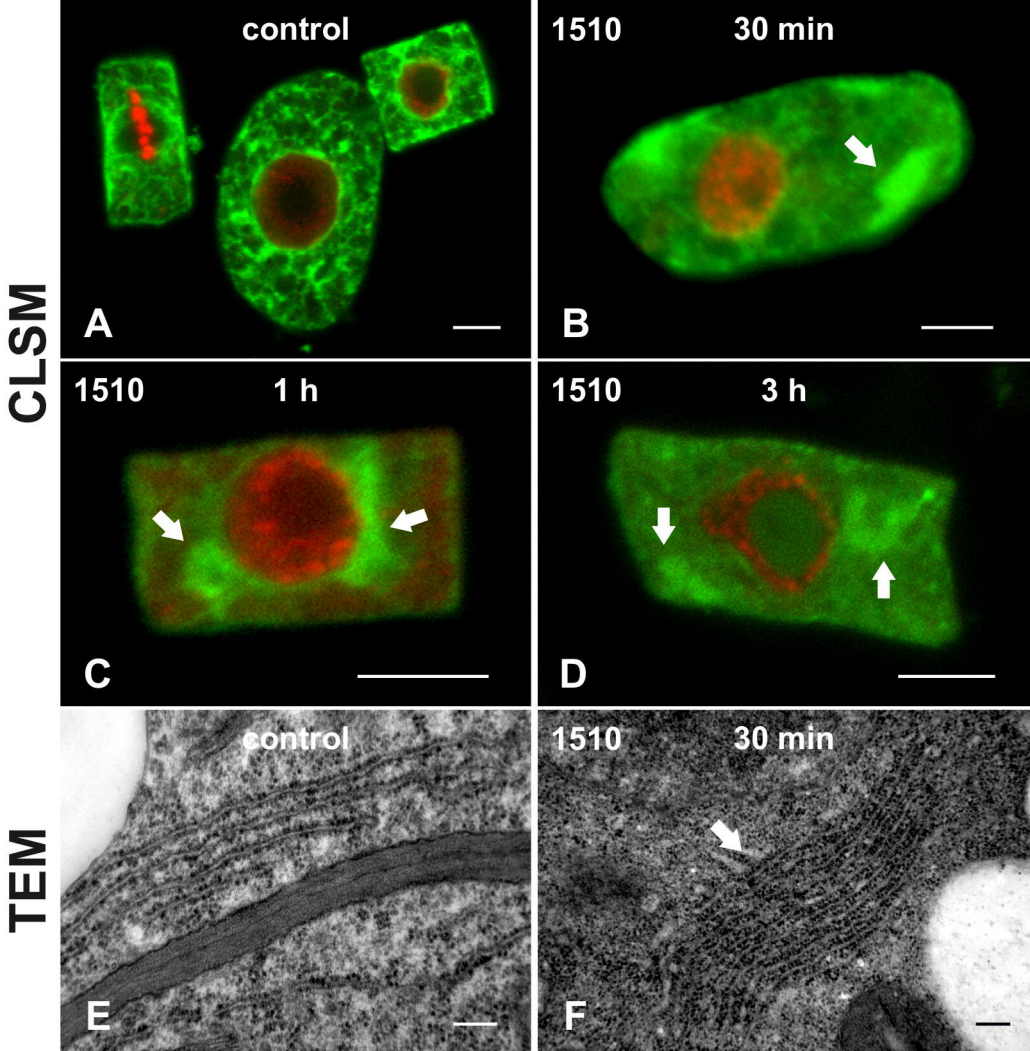
CLSM
control
A
1510
30 min
B
1510
1 h
C
1510
3 h
D
TEM
control
E
1510
30 min
F

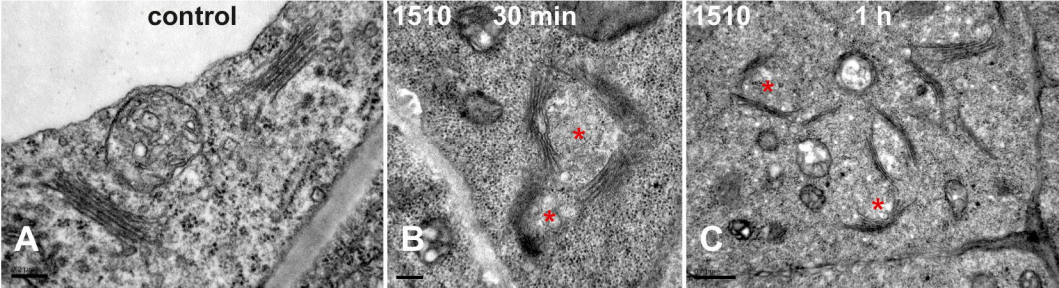
control
A
1510
30 min
B
1510
1 h
C